ANNALI DI GEOFISICA, VOL. XXXVII, N. 6, December 1994

Source mechanisms and near-source wave propagation from broadband seismograms

Jean Virieux([1]), **Anne Deschamps**([1]), **Julie Perrot**([1]) **and Jaime Campos**([2])
([1]) *Institut de Géodynamique, UNSA, Valbonne, France*
([2]) *Département de Sismologie, IPGP, Paris, France*

Abstract
Recording seismic events at teleseismic distances with broadband and high dynamic range instruments provides new high-quality data that allow us to interpret in more detail the complexity of seismic rupture as well as the heterogeneous structure of the medium surrounding the source where waves are initially propagating. Wave propagation analysis is performed by ray tracing in a local cartesian coordinate system near the source and in a global spherical coordinate system when waves enter the mantle. Seismograms are constructed at each station for a propagation in a 2.5-D medium. Many phases can be included and separately analyzed; this is one of the major advantages of ray tracing compared to other wave propagation techniques. We have studied four earthquakes, the 1988 Spitak Armenia Earthquake (M_s = 6.9), the 1990 Iran earthquake (M_s = 7.7), the 1990 romanian earthquake (M_s = 5.8) and the 1992 Erzincan, Turkey earthquake (M_s = 6.8). These earthquakes exhibit in different ways the complexity of the rupture and the signature of the medium surrounding the source. The use of velocity seismograms, the time derivative of displacement, increases the difficulty of the fit between synthetic seismograms and real seismograms but provides clear evidence for a need of careful time delay estimations of the different converted phases. We find that understanding of the seismic rupture as well as the influence of the medium surrounding the source for teleseismically recorded earthquakes requires a multistop procedure: starting with ground displacement seismograms, one is able to give a first description of the rupture as well as of the first-order influence of the medium. Then, considering the ground velocity seismograms makes the fit more difficult to obtain but increases our sensitivity to the rupture process and early converted phases. With increasing number of worldwide broadband stations, a complex rupture description is possible independently of field observations, which can be used to check the adequacy of such complicated models.

Key words *seismology – waveform – teleseismic earthquake – source analysis*

1. Introduction

Around the world, new seismic instruments have been installed for studying earthquakes and seismic wave propagation. These instruments allow the recovery of the ground motion in a broad frequency window without any saturation of the signal over a dynamic range of 10^8. Since the first installation of these instruments in 1984 through different national networks (GEOSCOPE, IRIS, MEDNET, and others...), seismic records for many earthquakes have been available to the scientific community.

These seismograms contain propagation information in a large frequency window now often reaching the impressive VBB window from 100 s down to 0.02 s. Moreover, in spite of field conditions, the broad spectrum is specified with confidence for these instruments,

making careful analysis of the ground motion possible.

As soon as records of world-wide networks became available, the understanding of the body wave amplitude for seismograms focused the attention of many researchers on structural analysis (Given and Helmberger, 1980; Paulssen, 1988), earthquake studies (Kikuchi and Kanamori, 1982; Kikuchi *et al.*, 1993) or both (Helmberger, 1968; Ruff, 1980; Owens and Crosson, 1988). We do not intend in this paper to give an overview of the improvements in seismic instrumentation, but one has to be aware that these first instruments, coming essentially from the WWSSN Long-Period network, have an instrument response which controls the shape of the seismogram: the recovery of the actual ground motion has always been a challenge to seismologists. In spite of these inherent technological difficulties, fitting the shape of body waves critically constrains both the focal mechanism and the depth of an earthquake for stations at distances between 30° up to 90° from the source (Ruff, 1980) for tectonic interpretation from these estimated parameters of earthquakes). The nearly homogeneous transparent structure of the mantle at long periods makes available information on a local earthquake process at far distances. For the nearest stations, wave propagation complications inside the upper mantle known as triplications must be included, leading to precise models of the upper mantle as below Europe (Paulssen, 1988; Papadimitriou, 1988).

As the quality of seismic records increases, more information concerning both earthquake ruptures and structural elastic properties encountered during propagation can be extracted. Unfortunately, distinguishing between the real source or an image by a given structure is difficult, especially in the source area where both wave excitations and wave conversions are intimately combined. Moreover, structures in tectonic areas are often complex, requiring more realistic wave propagation tools than those previously available. Azimuthal distribution of recorded stations provides an opportunity to distinguish source effects from local source propagation effects. Discrimination of amplifications beneath stations is somewhat easier, although their precise analysis would require local dense seismic networks (such as NORSSAR, NARS, TERRAscope). Phases observed on many stations are likely to come from the source area. In this paper, we shall concentrate our attention on interpretation of these near-source phases. We disregard possible hypothetical conversions on mantle heterogeneities observed on a given azimuthal range in this paper which are still at a debating level.

After a presentation of tools to synthesize seismograms in more and more realistic Earth models, we shall illustrate the possible contributions from source ruptures and from local propagation around the source using several recent earthquakes where many broadband seismograms are available.

The first earthquake we investigate is the Spitak, Armenian earthquake of 1988 (M_s = 6.9) which presents a complex rupture initiation, as inferred from both available broadband records and field observations. The Iranian earthquake of 1990 (M_s = 7.7) is an example of complex rupture described by broadband data with almost no information used from the field. The Rumanian earthquake of 1990 (M_s = 5.8) in the Vrancea region at a depth of 90 km is a good example of a simple source mechanism. Large-amplitude anomalies at particular azimuths is the unambiguous signature of complex wave propagation near the source. Finally, the Erzincan earthquake of 1992 (M = 6.2) at shallow depth provides an example of effects of local sedimentary basins interacting with a complex rupture process.

2. Wave propagation

Computation of seismic waves generated by a given discontinuity of displacement (slip) over a fault comes from the representation theorem (Aki and Richards, 1980) which gives the displacement $\boldsymbol{R}$ at the station $\boldsymbol{x}$ from the slip or dislocation $\Delta\boldsymbol{u}$ over the fault surface S. The component of the displacement along the n direction for a slip along the i direction is given by

$$R_n(\boldsymbol{x}, t) = \int \int_{\Sigma} \Delta u_i(\xi, t)\, n_j\, c_{ijpq} \star \frac{\partial}{\partial \xi_q} G_{np}\, d\Sigma \tag{2.1}$$

where c_{ijpq} are the elastic coefficients and G_{np} is the n^{th} component of the Green function for an impulsive point source acting in the p direction. The convolution is denoted by the sign $\star$.

For a force F_0 applied in the p direction at ξ, the Stokes expression (Aki and Richards, 1980) of the n^{th} component of displacement at $\boldsymbol{x}$ is the convolution $F_0 \star G_{np}$. The spatial derivative along the q direction introduced in the representation theorem (2.1) can be explained with an equivalent double couple or, more precisely, as a sum of double couples acting over the fault plane. We might consider an elementary double couple defined by (p, q) single force couples. In the general case, nine double couples exist. The strength of these double couples are $\Delta u_i(\xi, t)\, n_j\, c_{ijpq}$ per unit area. We can define the moment density tensor with

$$m_{pq} = \Delta u_i(\xi, t)\, n_j\, c_{ijpq} \tag{2.2}$$

and write the representation theorem (2.1)

$$R_n(\boldsymbol{x}, t) = \int \int_{\Sigma} m_{pq} \star \frac{\partial}{\partial \xi_q} G_{np}\, d\Sigma\,. \tag{2.3}$$

For an isotropic medium, the moment density tensor reduces to the simple expression

$$m_{pq} = \mu\,(n_p\, \Delta u_q + n_q\, \Delta u_p) \tag{2.4}$$

where μ is the shear modulus. If a horizontal fault is defined by the normal (0, 0, 1) with a slip Δu_x along the x direction, the moment density tensor reduces to a single number $\mu \Delta u_x$ along the x direction, which leads to the seismic moment once integrated over the fault surface.

How the slip is computed over the entire fault is a very difficult problem which must take into account laws of fracture mechanics. We might expect that waves emitted from one point on the fault will be diffracted by other points on the fault. The knowledge of this interaction is not necessary for computing the displacement everywhere as soon as we know the slip on the fault: this is the surprising result expressed in eq. (2.1). For this so-called kinematic approach, one describes the spatio-temporal variation of the slip and one computes seismic waves at specified stations. Many models have been designed with more or less realistic features. For example, the Haskell model (Haskell, 1964, 1966, 1969) is one of the simplest kinematic models considered in seismology. We are not sure that the specified geometry and excitations of the slip are compatible with any mechanical laws governing the rupture process. Other authors in this issue address this more difficult problem.

For teleseismic studies, the finite fault plane might be considered as a point source: waves emitted by the different points of the fault are nearly in phase and we may consider a system of couples with a moment tensor M equal to the integral over the fault surface of the moment density tensor:

$$M_{pq} = \int \int_{\Sigma} m_{pq}\, d\Sigma \tag{2.5}$$

leading to a very condensed expression for the representation theorem

$$R_n(\boldsymbol{x}, t) = M_{pq} \star G_{np,\,q} \tag{2.6}$$

with an obvious notation for spatial derivative. For planar fault surfaces, this system of couples reduces to the well-known representation of double couples of earthquakes. The first couple comes from the failure on the fault while the second one, orthogonal to the first, is the reaction of the medium (Burridge, 1976).

For this point source $\boldsymbol{x}_0$ approximation, the displacement is often condensed in one formula expressing the seismogram $R(\boldsymbol{x}, t)$ as a convolution of the source term $S(\boldsymbol{x}_0, t)$, the propagation term $G(\boldsymbol{x}, \boldsymbol{x}_0, t)$ and the station or instrument term $I(\boldsymbol{x}, t)$. The convolution can

be written

$$R(\boldsymbol{x}, \boldsymbol{x}_0, t) = I(\boldsymbol{x}, \boldsymbol{x}_0, t) \star G(\boldsymbol{x}, \boldsymbol{x}_0, t) \star S(\boldsymbol{x}_0, t). \tag{2.7}$$

The seismogram shown in fig. 1 provides clear evidence of a signal transported from the source to the station with additional conversions due to the Earth's structure. We are interested in how to interpret them. This raw broadband seismogram will be analyzed later on to illustrate the capability to recover the true ground motion.

The Earth is a translucent body and the signal emitted by the seismic source is partly preserved during propagation over thousands of kilometers. In particular, the mantle propagation can be considered in many studies as a propagation in a rather homogeneous medium over the frequency range used in teleseismic studies from 1 Hz down to 0.01 Hz with an anelastic attenuation described in terms of a quality factor Q for the selected body phase. Consequently, waves propagate in heterogeneous media around the source and around each station. The geological context of each station is different and might provide particular

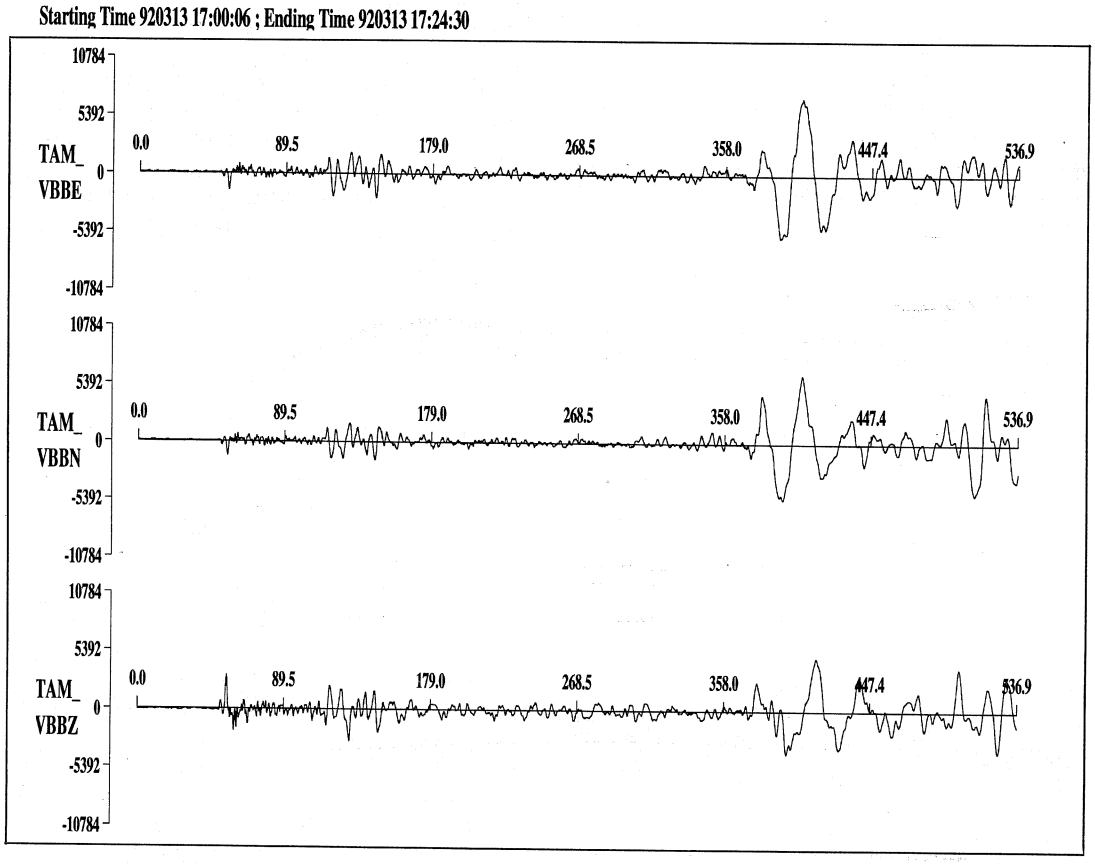

Fig. 1. The broadband seismogram recorded at station TAM -GEOSCOPE- for the Erzincan earthquake: the three components are displayed. Different phases can be identified and associated to structures inside the Earth.

features on individual seismograms while the source structure signature might be seen on many seismograms. We think it is possible to discriminate source signature observed on many seismograms with particular wiggles associated to local station propagation.

We may split the propagation term into three parts: the propagation near the source $G_S(\boldsymbol{x}, \boldsymbol{x}_0, t)$, the propagation into the mantle $G_M(\boldsymbol{x}, \boldsymbol{x}_0, t)$ and the propagation near the receiver $G_R(\boldsymbol{x}, \boldsymbol{x}_0, t)$. We reduce the third propagation term G_R to the influence of the free surface in this approach focused on analysis of earthquakes source mechanisms. This third term might be very important for seismic risk for example. The second term G_M can be modelled very simply by using wave propagation inside homogeneous media, while the first term G_S is the operator we want to study in association with the source term $S(\boldsymbol{x}_0, t)$. For locally recorded earthquakes, it is very difficult to separate source effects and wave propagation around the source. For teleseismically recorded earthquakes, partial discrimination can be performed using station azimuth coverage, which samples different parts of the medium around the source.

2.1. *Source mechanism*

The seismic radiation of waves for a dislocation can be regarded as the response of a double-couple with a seismic moment $M(t)$ (scalar quantity) in a homogeneous medium which gives the P phase displacement u^P, the shear horizontal displacement u^{SH} and the shear vertical displacement u^{SV}

$$u^P(\boldsymbol{x}, \boldsymbol{x}_0, t) = \mathcal{R}^P \frac{1}{4\pi\rho\alpha^3} \frac{1}{r} \dot{M}\left(t - \frac{r}{\alpha}\right) \boldsymbol{i}$$

$$u^{SV}(\boldsymbol{x}, \boldsymbol{x}_0, t) = \mathcal{R}^{SV} \frac{1}{4\pi\rho\beta^3} \frac{1}{r} \dot{M}\left(t - \frac{r}{\beta}\right) \boldsymbol{j}$$

$$u^{SH}(\boldsymbol{x}, \boldsymbol{x}_0, t) = \mathcal{R}^{SH} \frac{1}{4\pi\rho\beta^3} \frac{1}{r} \dot{M}\left(t - \frac{r}{\beta}\right) \boldsymbol{k} \qquad (2.8)$$

where ρ, α and β are density, P-wave velocity and S-wave velocity at the source, respectively. In addition, r is the distance to the source, while the local reference frame $(\boldsymbol{i}, \boldsymbol{j}, \boldsymbol{k})$ is described in fig. 2. The seismic moment appears through its time derivative denoted by a dot. The factor $\rho\alpha^2$ for P waves ($\rho\beta^2$ for S waves) is simply the appropriate elastic factor to give the displacement response of the medium to a given force. The factor 4π says that it is a point source along one direction which has to be normalized with respect to the whole sphere. The additional factor α for P waves (β for S waves) comes from the double-couple derivation as well as the time derivative of the moment.

Radiation patterns $\mathcal{R}^P$, $\mathcal{R}^{SV}$, $\mathcal{R}^{SH}$ define the amplitude of waves emitted by the double-couple towards the station. They give the geometry of the fault plane, *i.e.* the focal mechanism through the strike, dip and slip angles (ϕ, δ, λ) as defined in fig. 2 with respect to the ray, which leaves the hypocenter towards the station. Let us denote γ the unit direction of this

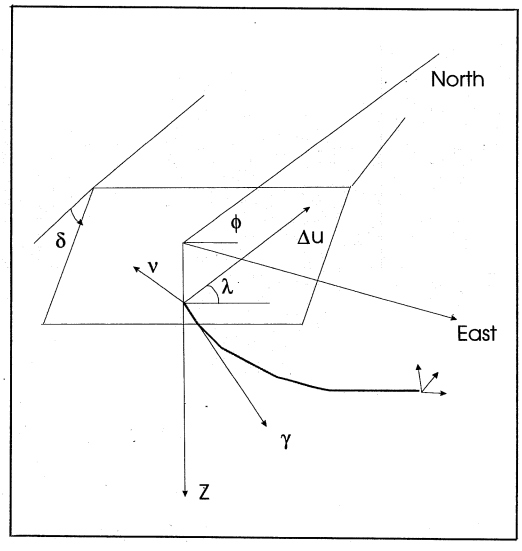

Fig. 2. The three-dimensional geometry of the seismic fault plane: the slip occurred in the direction λ while the fault is defined by its azimuth ϕ and and its dip δ.

ray which is equal to $\boldsymbol{i}$ for a homogeneous medium. The radiation pattern might be viewed as the deformation of a unit excitation sphere by the very specific directivity of the seismic double-couple (see fig. 3). The radiation pattern is directly deduced from the moment tensor definition (2.4) and might be expressed using bracket conventions very convenient for tensors of second order

$$\begin{aligned} \mathcal{R}^{\mathrm{P}} &= <\boldsymbol{i}|\dot{\boldsymbol{M}}|\gamma> \\ \mathcal{R}^{\mathrm{SV}} &= <\boldsymbol{j}|\dot{\boldsymbol{M}}|\gamma> \\ \mathcal{R}^{\mathrm{SH}} &= <\boldsymbol{k}|\dot{\boldsymbol{M}}|\gamma> \end{aligned} \qquad (2.9)$$

2.2. *Wave propagation around the source*

The very first influence of the medium around the source on waves leaving the source is from the free surface. Reflected P phases produced by P and S phases emitted from the source give good control on the depth of the hypocenter. These phases are denoted pP and sP. They are leaving the focal sphere through points other than the P wave. Let us denote the take-off angle of P waves as i_α and of S waves as i_β. In a homogeneous medium, the take-off angle becomes $\pi - i_\alpha$ for the pP phase and $\pi - i_\beta$ for the sP phase. For a heterogeneous medium, these angles are quite different. These waves are then propagating as P waves up to

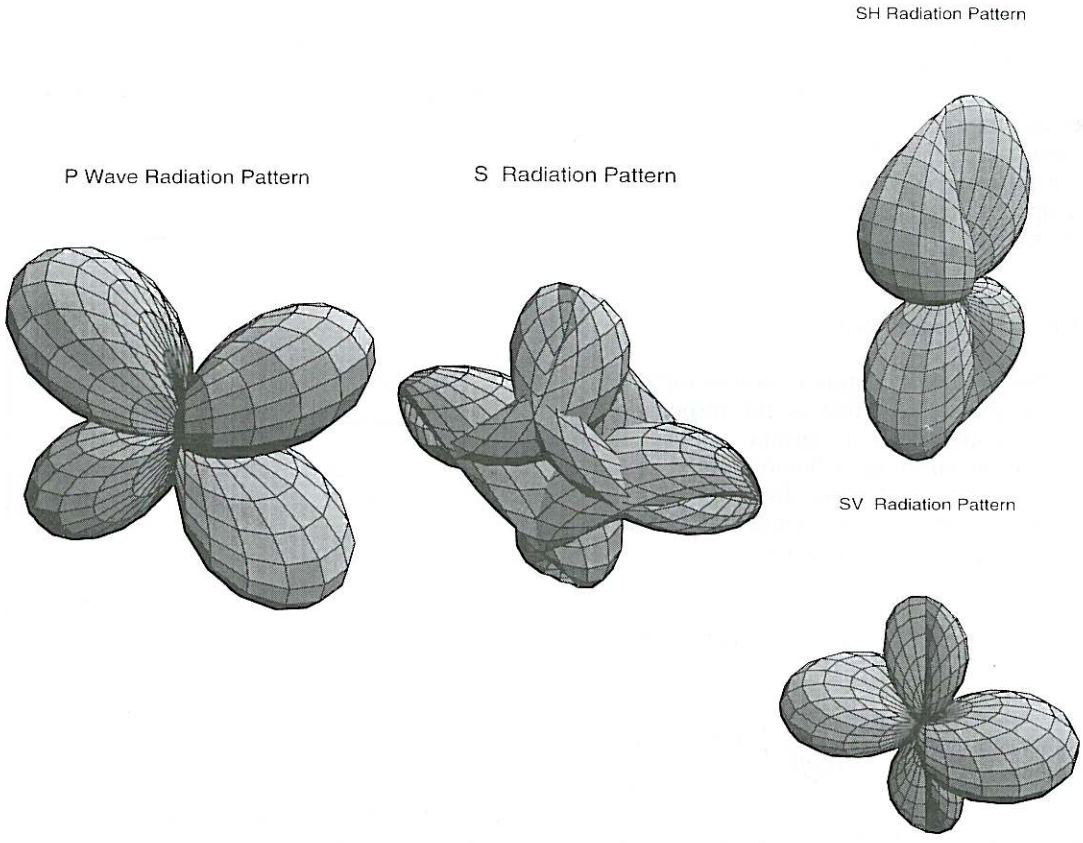

Fig. 3. Diagram for P-wave and S-wave radiation patterns: the S-wave radiation pattern can be projected in order to obtain SH-wave pattern or SV-wave pattern separately.

the station and the same tools can be used for the propagation. A simple review has been given by Okal (1992) with a global expression including these three waves (*P*, *pP*, *sP* phases) in a spherical Earth.

By fitting these additional phases at teleseismic distances, we increase the sampling of the focal sphere and better constrain the focal mechanism of earthquakes. Using WWSSN LP instruments, seismologists have been able to study earthquakes occurring around the world for the last thirty years.

With more and more sensitive instruments, additional features coming from the source area have been taken into account. Seafloor bathymetry as well as sedimentary layers have been taken into account even for the WWSSN LP stations with ray tracing (Wiens, 1989) or with finite difference propagation (Okamoto and Miyatake, 1989). Detailed modelling of teleseismic wave shapes for direct *P* and *S* waves as well as for converted waves must be performed in order to fit observed seismograms.

Recently, it has been possible to reproduce the complex signal for nuclear explosions in the Yucca Flat Basin recorded at teleseismic distances in France (Gaffet, 1995). The critical point for successfully modelling wave forms is the precise knowledge of the medium around the source. Any missing feature around the source would strongly modify the incoming signal at specific stations.

Although techniques for propagating the entire seismic wave field without any approximations are interesting in the complex medium surrounding the source, we preferred to use ray tracing for three reasons. The asymptotic approximation is the same along the entire path between the source and the station and ray tracing is a perfect tool for interpretation and for fast calculation. Although azimuthal velocity variations require 3-D ray tracing (Kendall and Thomson, 1993), we performed 2-D ray tracing as a first investigation of the medium structure around the source. With an increasing number of broadband stations, it will be possible to consider true 3-D propagation.

Rays are traced around the source using a local Cartesian coordinate system. We solve both the kinematic and paraxial ray tracing system for initial conditions, which gives us the ray information needed to compute the travel-time and the amplitude of the seismic signal at any point along the ray. The detailed description of the parameters to trace rays as the numerical solver, the sampling parameter, velocity or interfaces descriptions can be found in Farra *et al.* (1989) or in Virieux and Farra (1991) and is summarized for teleseismic studies by Perrot *et al.* (1994).

Once we have left the source area, we switch to the global frame located at the center of the Earth at a constant depth. The global frame is defined by a spherical coordinate system which is more adapted for solving ray tracing equations, especially around the center of the Earth (Červený and Janský, 1983). The constant-depth surface is a plane in the local Cartesian coordinate system and a shell of constant radius in the global spherical coordinate system (see fig. 4). On this so-called hybrid

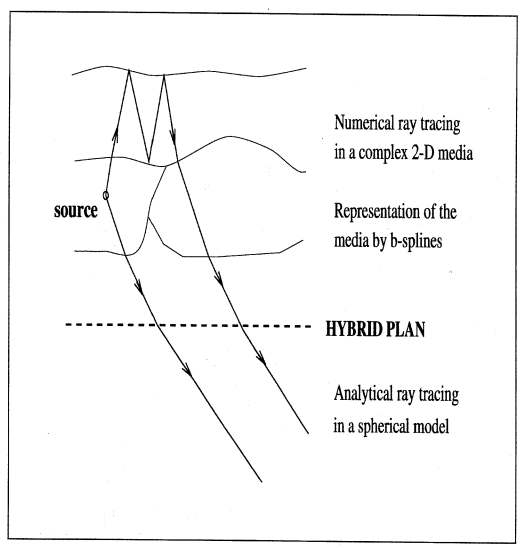

Fig. 4. Schematic description of the medium around the source. Above the hybrid plane, the ray tracing is performed numerically in laterally varying structures while, below the hybrid plane, the ray tracing is performed analytically in a stratified medium.

plane, we compute ray quantities needed for continuing ray tracing up to the station where synthetic seismograms are constructed.

By anticipation, let us glance at perturbations from a complex medium around the source. For an interplate earthquake near an east-dipping zone, eastern stations are sensitive to the subduction zone while western stations do not see this laterally varying structure (fig. 5). Additional phases like the *pwP* phase (a reflection from the water-air interface) or *pwwP* phase (a double reflection within the water layer) produce noticeable amplitude variations in the seismogram. This difference is still present after propagation to the teleseismic station (fig. 6).

2.3. *Wave propagation through the mantle*

When waves enter into the mantle, we might assume that the Earth is of spherical shape and only radially heterogeneous. The already perturbed wave front will continue to deform in a more gentle way. Again, this heterogeneous medium would require complex tools for wave propagations. Spectral methods such as the Cagniard-De Hoop method (Helmberger, 1968), reflectivity method (Fuchs and Müller, 1971) or generalized ray theory (Chapman, 1978), which requires integration over wave number or slowness parameter, gives significant contributions for a number of these slowness parameters or, in other words, for a few

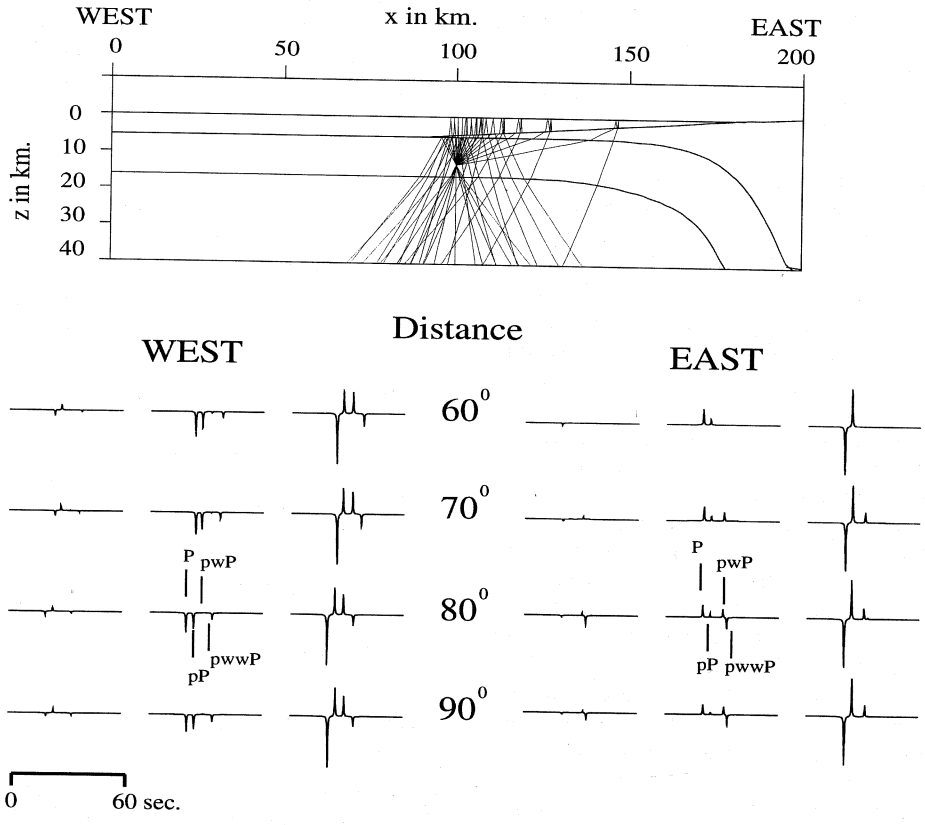

Fig. 5. Description of the Green function for complex medium around the source with associated ray tracing: west and east stations will record quite different seismograms.

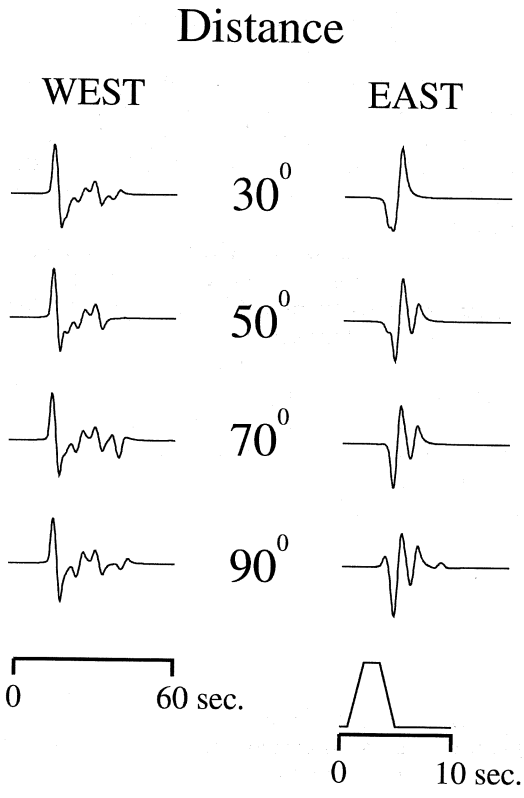

Fig. 6. Synthetic seismograms for stations on the west and east sides obtained by convolution of the Green function, attenuation factor and instrument response.

rays. Therefore, geometrical ray theory is enough to analyze the body waves as long as the station can be reached by rays. With a systematic search, we track any slowness parameter and the associated ray with a significant contribution at the selected station.

The ray tracing through the whole Earth is performed in the spherical coordinate system using analytical expressions of (Červený, 1983). This ray tracing gives stable and precise estimation of the amplitude.

The different quantities computed in the local Cartesian frame and in the spherical reference frame are combined to give ingredients for computing the Green function. Assuming an invariance along the axis perpendicular to the 2-D medium we consider, we estimate the geometrical spreading $J_{2.5D}$ for this so-called 2.5D geometry from the geometrical spreading J_{2D} computed during the ray tracing (Perrot *et al.*, 1994).

The Green function which includes the effects around the source and the propagation in the mantle will be written

$$G(\boldsymbol{x}, \boldsymbol{x}_0\, t) = C \frac{\sqrt{\rho_0\, v_0}}{\sqrt{\rho\, v}} \frac{e^{i\pi k m a h/2}}{\sqrt{|J_{2.5D}|}} \mathcal{D}(t\text{-}T) \tag{2.10}$$

where T is the travel-time of the selected wave, C is the product of refraction/reflection coefficients and *kmah* is the kmah index. Density and velocity are denoted ρ_0 and v_0 at the source and ρ and v at the station. The Green function G depends on the selected wave. The function $\mathcal{D}(t)$ is the analytical function $\delta(t) - i/\pi t$ of the Dirac function $\delta(t)$.

In order to take the attenuation into account, the spectral amplitude must be decreased by a factor $\exp(-\omega t/2\mathcal{Q})$ where t is the travel time of the phase. The factor $t^* = t/\mathcal{Q}$ has been found empirically constant, practically independent of distance. As the distance increases, the travel time increases while the wave goes deeper in mantle areas where $\mathcal{Q}$ is higher. The single parameter t^* takes a value of 1 s for P waves and 4 s for S waves (Carpenter and Flinn, 1965; Anderson and Hart, 1978). We must add this influence to our estimation of the Green function.

2.4. *Station response*

The first influence comes from the free surface where the instrument is installed. The recorded motion includes the incident wave and the reflected wave. The factor we must take into account depends on the incidence angle of the ray through reflection coefficients. Combining this term with the instrument response I provides us with the complete

recorded signal which can be written

$$R(\boldsymbol{x}, \boldsymbol{x}_0\, t) = I(\boldsymbol{x}, \boldsymbol{x}_0\, t) \star \mathcal{Q}(\boldsymbol{x}, t) \star$$

$$\star\ \mathcal{R}\, C \frac{\sqrt{\rho_0\, v_0}}{\sqrt{\rho\, v}} \frac{e^{i\pi k m a h/2}}{\sqrt{|J_{2.5D}|}} \mathcal{D}(t\text{-}T) \star \frac{\dot{M}}{4\pi\rho_0}\,. \tag{2.11}$$

In this paper, we do not take into account effects other than free surface below stations neglecting in the seismogram phases coming obviously from the Earth structure below the station. The generation of waves by the local Earth structure can strongly modify the signal and has its own importance. Local 3-D networks of stations are and will be the efficient way to analyze these waves and will reveal the presence of anomalous bodies which diffract them. We might consider in the future more realistic media under recorded stations.

One important feature we want to stress is the capability of new seismographs to provide the ground displacement over a wide frequency window.

The signal extracted from the vertical seismogram of fig. 1 is recorded in counts and is displayed on top of fig. 7. One can numerically integrate this time signal, which gives the second record of fig. 7. These signals have no meaning with respect to physical quantities. If we introduce the instrument response, we can recover both velocity and displacement of the ground from the first record. We find that the velocity looks like the raw data, while the dis-

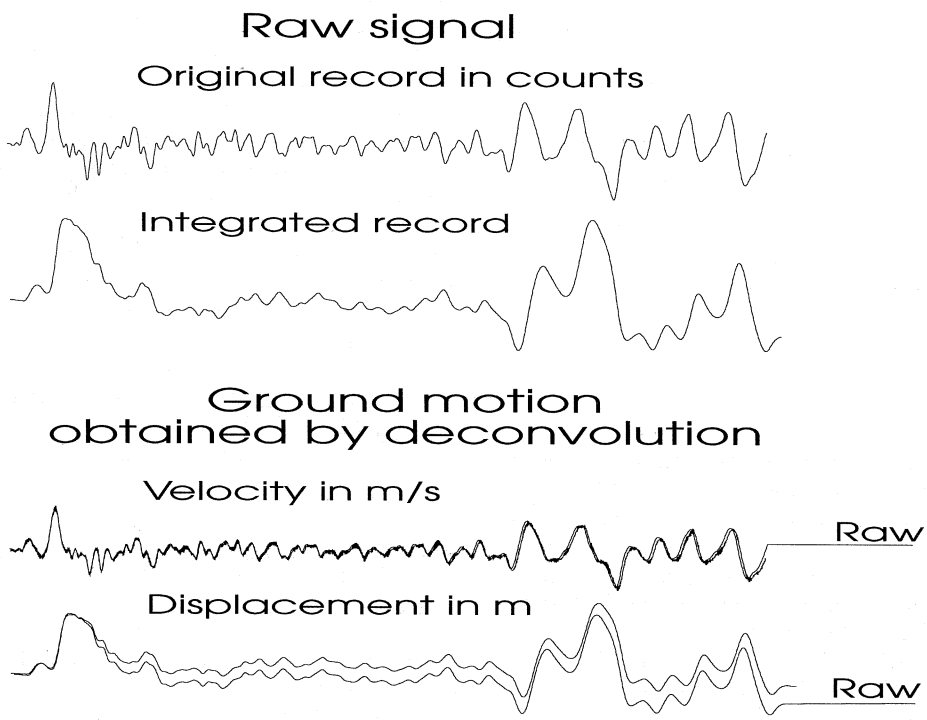

Fig. 7. Raw and deconvolved seismograms at station TAM- GEOSCOPE- for the Erzincan earthquake. These seismograms are extracted from fig. 1. The numerical integration of raw data in counts (top) will show a seismogram similar in shape to the true displacement obtained by integrating the deconvolved velocity (bottom).

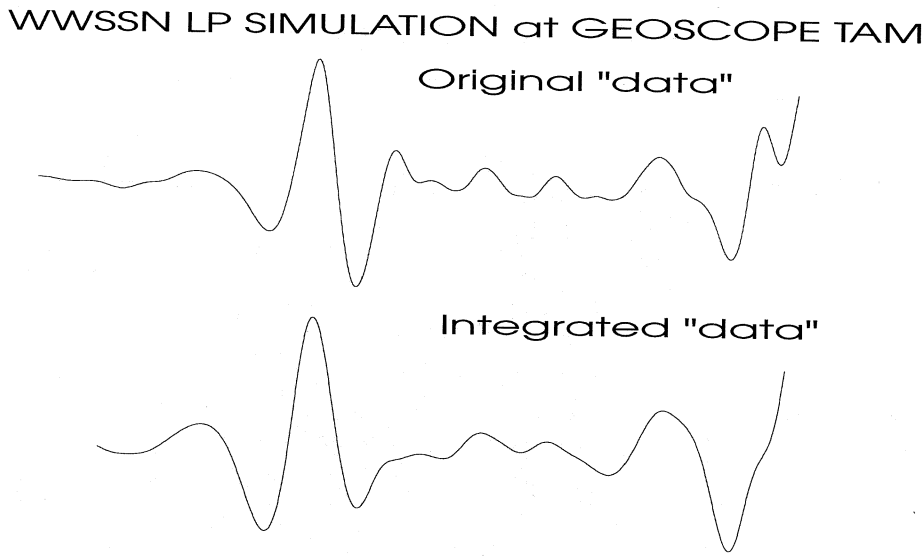

Fig. 8. Simulated WWSSN LP seismograms at TAM- GEOSCOPE- station: we show the reconstructed LP data as well as the deduced integrated signal. The shape of seismograms is dominated by the instrument response.

placement looks like the original integrated record except for a very low frequency component, which is easy to cancel. In other words, the instrument response is flat with respect to velocity; this is why these instruments are sometimes called velocimeters.

In order to appreciate the quality of these seismograms, let us present in fig. 8 the velocity signal with a filter of a WWSSN LP seismogram on the top and the hypothetical WWSSN LP displacement seismogram on the bottom. The difference between velocity and displacement is overshadowed by the instrument response which dominates the shape of the signal and which has made the success of WWSSN network for studying nuclear explosions and earthquakes. Inversions of wave shapes were similar using either ground velocity or displacement recorded by these seismographs. We see that broadband seismograms present very different shapes for displacement and velocity quantities. This change in the frequency content has an increasing role to play when details of the rupture and propagation are looked for.

Let us start our review of body waves modelling by the the Spitak Earthquake of December 7, 1988, four years after the first installation of broadband instruments.

3. The Spitak earthquake of December 7, 1988 (M_S = 6.9)

This earthquake was one of the first earthquakes to have a well-constrained azimuthal coverage by broadband stations (see fig. 9) and displaying a complex rupture process. This earthquake was located very close to the surface, and the nearby city of Spitak was almost completely destroyed by this event (Cisternas *et al.*, 1989). Focal mechanisms obtained by different methods give a thrust mechanism with a nodal plane dipping towards the North in agreement with the tectonics expected near the Pambak-Sevan fault (Philip *et al.*, 1989).

Early studies, such as Cisternas *et al.* (1989), already show the complexity of the rupture, with a two-event model preceeded by a small precursor. Moreover, separation be-

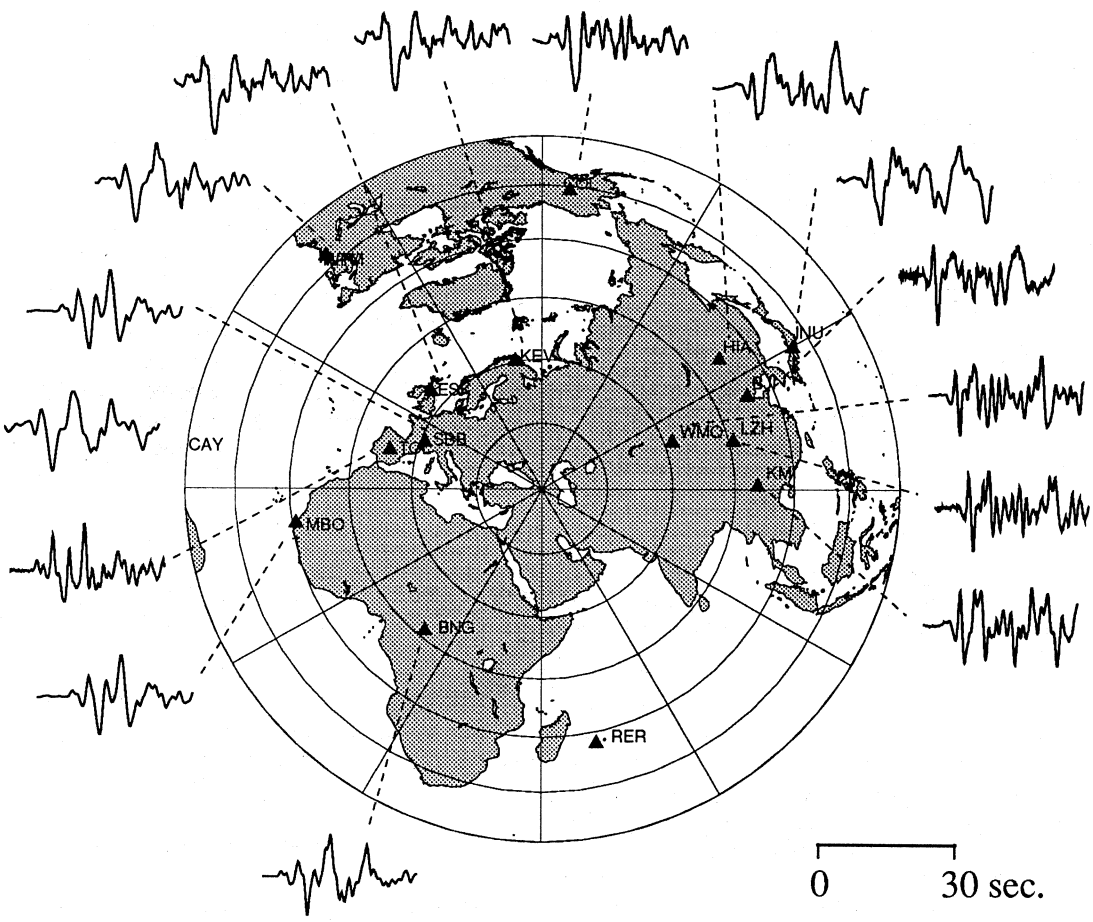

Fig. 9. Unscaled broadband seismograms for the Spitak earthquake in order to show the available azimuthal coverage for this earthquake.

tween pulses is larger at the Chinese stations than at African, European and American ones as shown in fig. 9, suggesting that the rupture propagated from east to west. A more detailed analysis was made by Haessler *et al.* (1992) with an increased number of broadband data. By spectral analysis and seismogram deconvolution of raw data, they found that two shocks can be inferred directly from the data, with a time lag around 10 s. A recent work (Kikuchi *et al.*, 1993) also reports a complex rupture. In order to fit observed seismograms (fig. 10), these authors introduced a more complex three-segment fault model similar to those obtained by other authors (Pacheco *et al.*, 1989). These three segments are not deduced by seismogram analysis but come from field observations. The tectonic interpretation of this multi-event structure encounters difficulties: why is one of these events outside the aftershock zone, and how can we integrate its focal mechanism into the global tectonic scheme?

To solve these difficulties for seismo-tectonic interpretation, Haessler *et al.* (1992) proposed a model with five segments using information provided by aftershock analysis and ge-

ological observations. Each segment of the fault rupture was discretized by a sequence of point sources equally separated in time and space, assuming a rupture velocity of 2.9 km s^{-1}. The source-time function is even more complex than for the three-event model. The fit between observed $\boldsymbol{x}$ and calculated $\boldsymbol{y}$ seismograms (fig. 11) defined by $m = |\boldsymbol{x} - \boldsymbol{y}|/\boldsymbol{x}$ is not drastically better (0.61) than for the three-event model (0.68), but the final tectonic interpretation inferred from this model is much more consistent with field observations than from the previous simpler three-event model.

The complexity of the inferred source mechanisms should not shadow the fact that real seismograms were low-pass filtered at 0.2 Hz. How can we obtain such detailed resolution of the rupture time process with such low-frequency content in the seismogram signal? Although the respective adequacy of the two different final models could be discussed, one should emphasize that the majority of main phases were explained by these rupture models, eliminating the need for a complex structure of the near-source medium. With broadband data, we were able to interpret this already complex seismic event.

We shall see now an even more complex rupture process with bilateral propagation for the Iranian earthquake of June 1990.

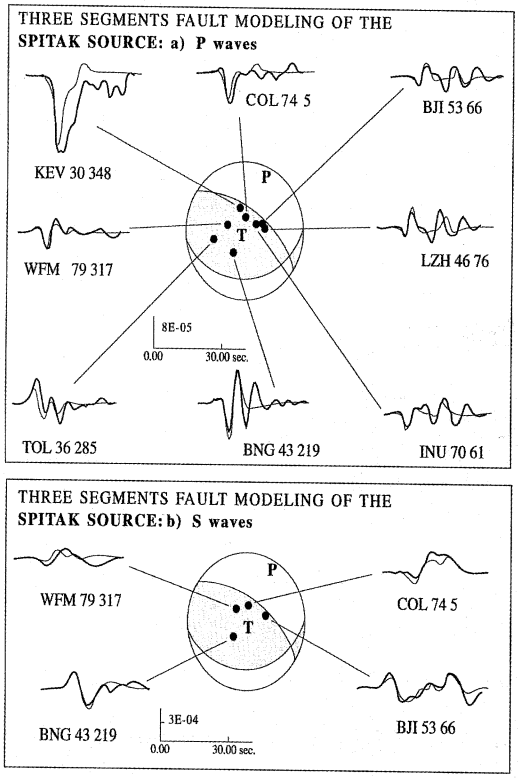

Fig. 10. Observed and synthetic seismograms for the three-event model of the Spitak earthquake from Haessler *et al.* (1992). The thin line is the synthetic signal while the thick one is the observed seismogram.

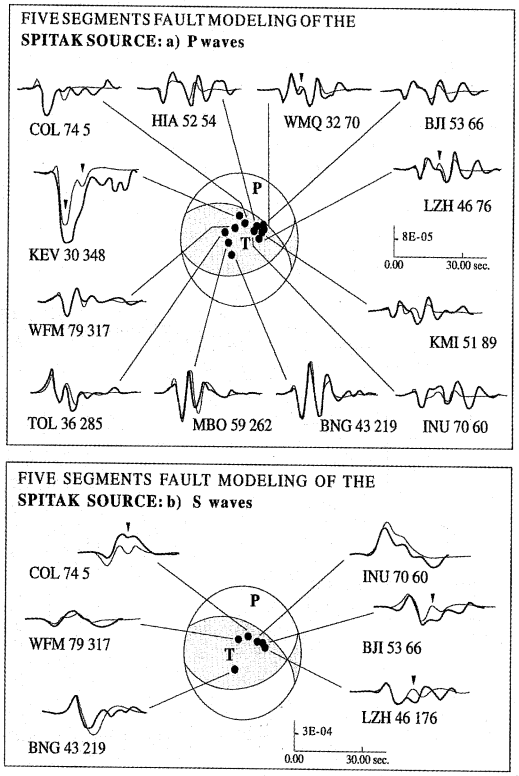

Fig. 11. Observed and synthetic seismograms for the five-event model of the Spitak earthquake from Haessler *et al.* (1992). The thin line is the synthetic signal while the thick one is the observed seismogram.

4. The Iranian earthquake of June 20, 1990 (M_S = 7.7)

A year and a half after the Iranian earthquake occurred, with increased azimuthal coverage of broadband stations (these two earthquakes occurred in the same area with respect to world-wide stations; see fig. 12). This strike-slip event again shows rupture complexity which has been studied by many authors: Campos *et al.* (1994) were able to define nine events over the first 25 s. These events describe a bilateral rupture with northwestern and southeastern propagation during the first ten seconds, reducing to a single, southeastern rupture propagation for the last part of the source excitation.

Again, to bring all records into the same frequency band, a Butterworth filter of order 3 was applied to displacement records between 0.01 Hz-0.2 Hz (periods from 100 s to 5 s). Moreover, for a proper weighting between stations, every record was converted to a seismogram hypothetically recorded at a 40° station with same azimuth and common gain.

The complexity of the source rupture is readily observed in fig. 13 where, as mentioned by Campos *et al.* (1994), a gradual change of polarity near station *HRV* is detected. The main pulse arrives 10 s later with a nodal plane passing near the station *TAM*, showing that a single focal mechanism could not explain the entire rupture process.

By considering more and more details of the rupture scheme, Campos *et al.* (1994) were able to invert the body wave data using a procedure (Nábělek, 1984) based on the maximum likelihood principle (Jackson, 1979; Tarantola and Valette, 1982).

For a first step, an inversion using a point source provides a satisfactory fit for *P* and *SH* waves as shown in fig. 14. The inverted focal mechanism is (ϕ = 301°, δ = 75°, λ = 4.8°) at a depth of 11.7 km. The seismic moment $M_0 = 1.05 \times 10^{20}$ Nm is released about 24 s from the first arrival. The initial *P* signals are well reproduced while unexplained later phases might be associated with crustal reverberations. The *SH* seismograms fit less successfully with significant amplitudes underestimated on the

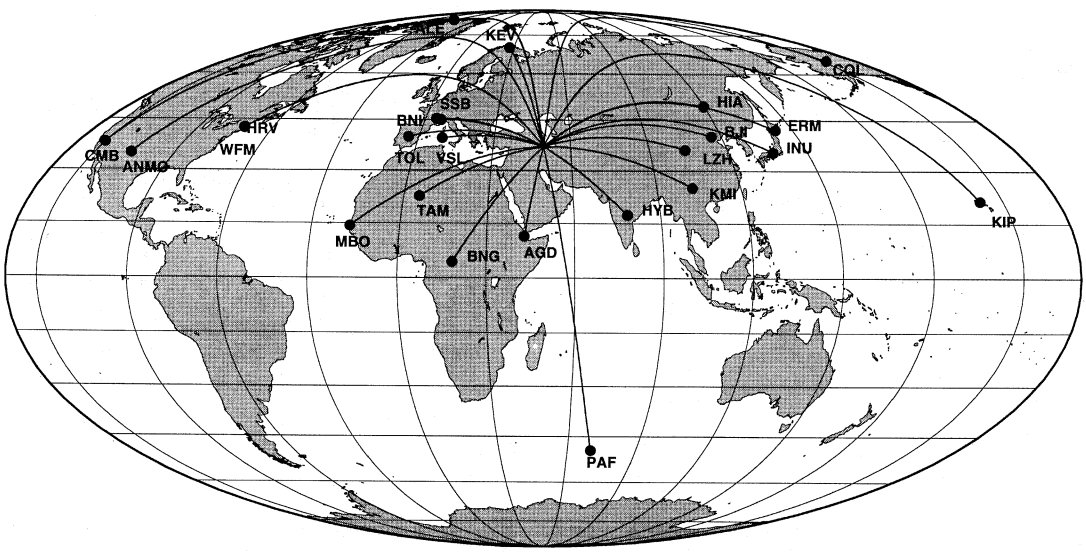

Fig. 12. Azimuthal coverage of broadband stations for the Iranian earthquake: see the increasing coverage with respected to the Spitak earthquake (fig. 9).

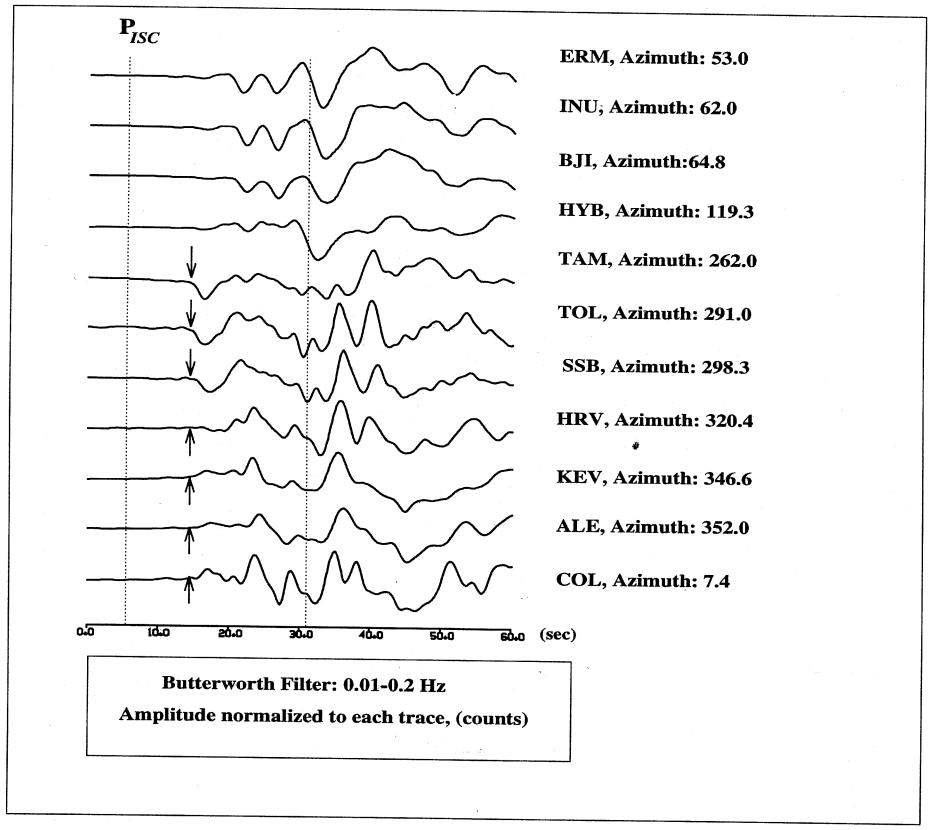

Fig. 13. Ground displacement for broadband *P* waves filtered in the frequency range 0.01 Hz - 0.2 Hz for the Iranian earthquake. Note the delay compared to the *P*-wave travel time published by the ISC Bulletin. A polarity change is pointed by vertical arrows.

East side and overestimated on the West side.

Including the directivity effect of a propagating source should improve the fit and a systematic exploration of the model space along the rupture azimuth axis and, then, along the velocity rupture axis led Campos *et al.* (1994) to a rupture azimuth 120° compatible with the point source focal mechanism and a rupture velocity of 2.5 kms^{-1}. Of course, each subevent has a simpler time function with a total duration of 4 s and a rise time of 2 s. Unfortunately, the fit was not reduced significantly with respect to the point-source solution. We might consider changes in the rupture velocity or in the focal mechanism of each subevent. We might also consider a bilateral propagation as Campos *et al.* (1994) did. This interactive multi-step procedure is required by the large number of parameters we consider for complex rupture. Nevertheless, the azimuthal coverage of this earthquake leads us to a reasonable model less based on field observations than the Spitak earthquake.

Assuming a bilateral propagation plotted in fig. 15 with 4 points on the west side (30 km) and 8 points on the east (60 km), Campos *et al.* (1994) inverted for focal mechanisms for each simple subevent and found a much better fit of seismograms (fig. 16) compared to the single point source model. Amplitudes of *P* waves as well as *SH* waves are better described with the

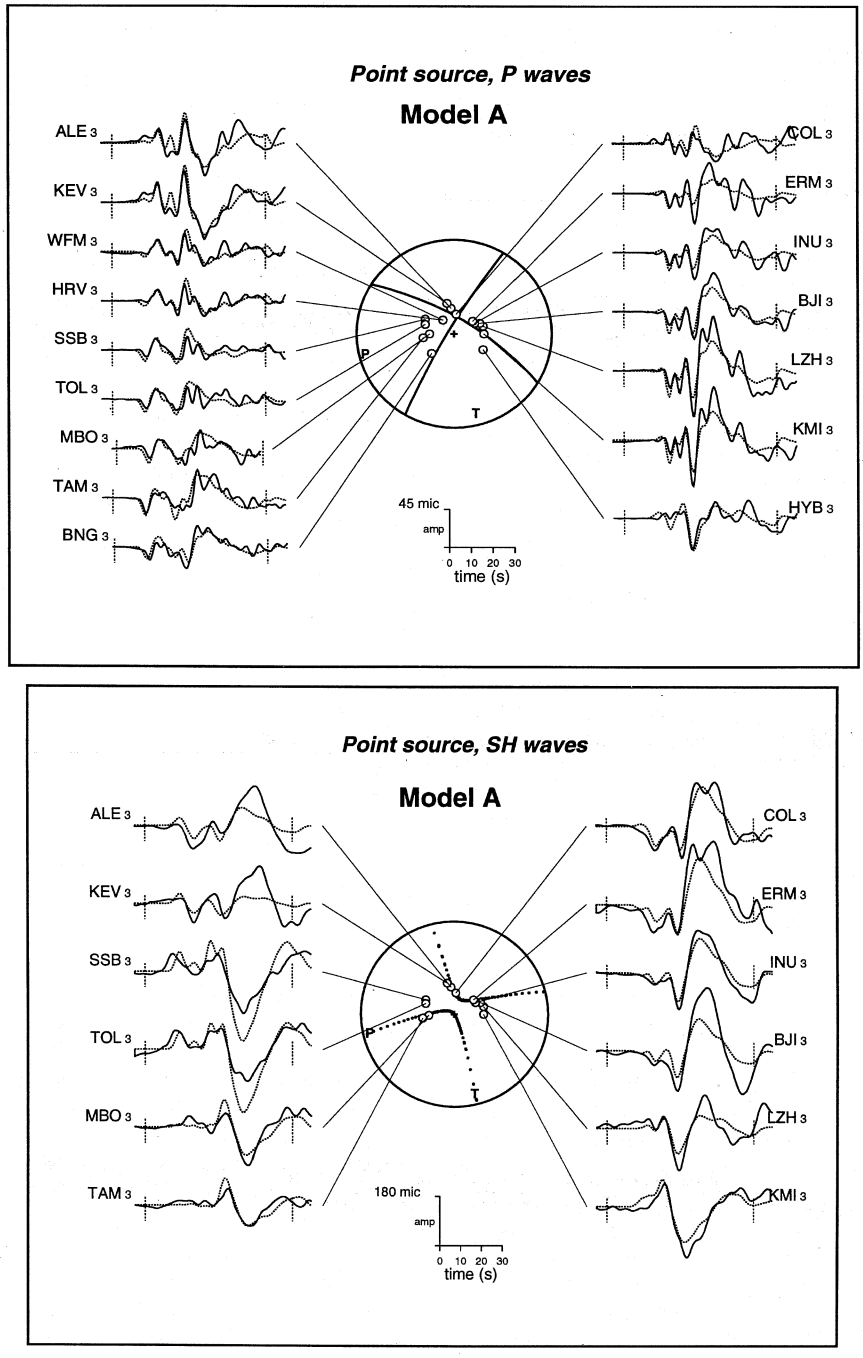

Fig. 14. Comparison of observed and synthetic *P* and *SH* seismograms for a point-source model for the Iranian earthquake.

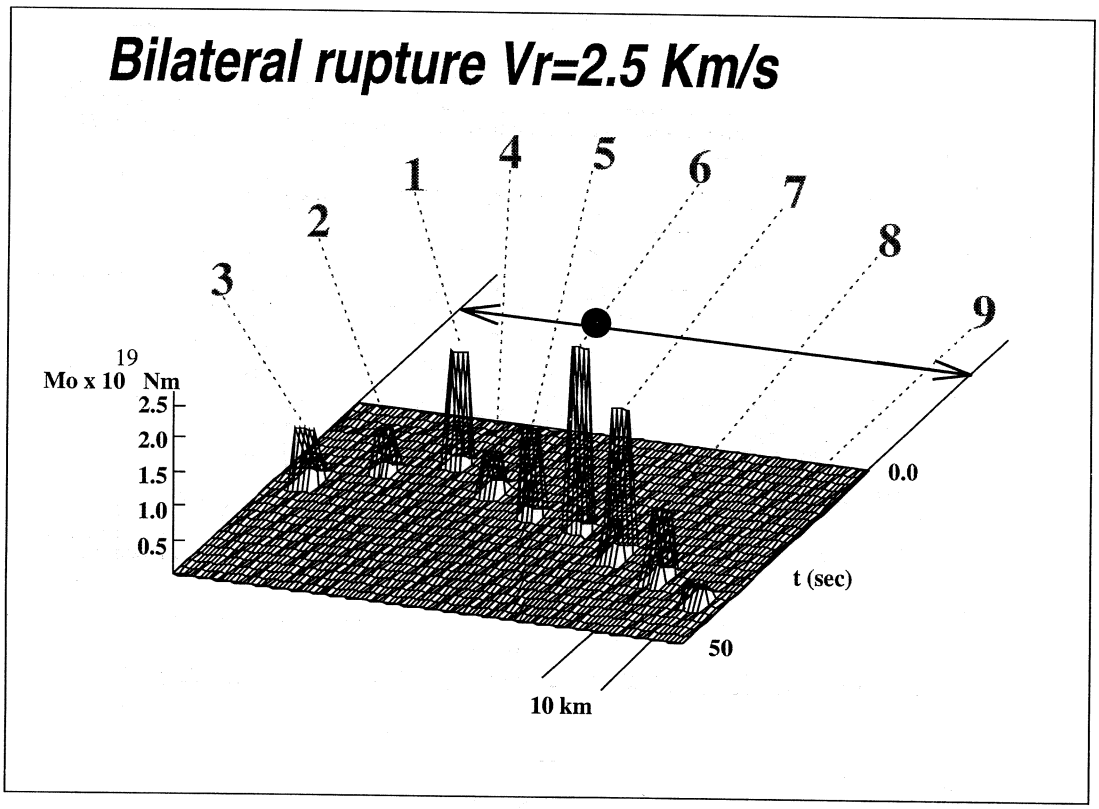

Fig. 15. Bilateral propagation of the rupture for the complex twelve-subevent model for the Iranian earthquake. The amplitude is proportional to the moment of each sub-event.

unexplained crustal phases still remaining. These phases were not included artificially in the source function because some stations did not see them.

Many restrictions exist on the inversion procedure and the iterative way to arrive at the final solution played a key role in the final model. Nevertheless, the improved fit of seismograms (fig. 16) can be easily distinguished and might convince us that a resolution of significant details of the slip distribution over the 100 km long fault has been reached.

Undoubtedly, lateral heterogeneities in the source region might affect these rather precise source models. Surprisingly, no clear early strong phases can be shown to be related to local source heterogeneities, at least on displacement seismograms. We might say again that the main feature of this earthquake is the dominance of a complex rupture process which is well analyzed by broadband data.

We shall describe now an earthquake with a relatively simple rupture that will display anomalous amplitudes, which can not be explained by the rupture process.

5. The Rumanian earthquake of May 30, 1990 (M_S = 5.8)

A magnitude 5.8 event occurred on May 30, 1990, in the Vrancea area at a depth of 90 km and was recorded on broadband stations.

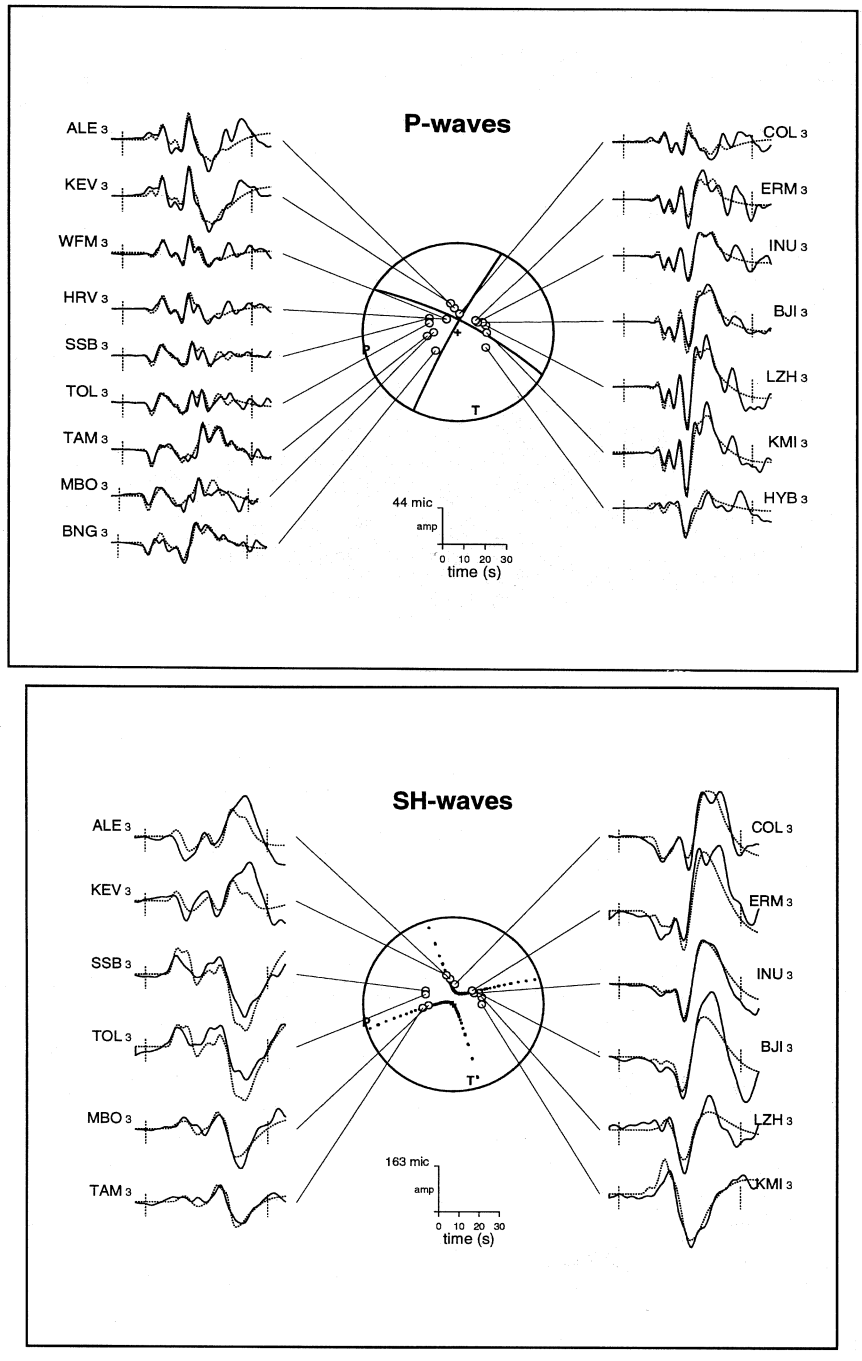

Fig. 16. Comparison of observed and synthetic *P* and *SH* seismograms for the complex twelve-subevent model for the Iranian earthquake. Compare with the seismograms of fig. 14 and note the increasing fit.

Again, we are still with approximately the same azimuth coverage with respect to the worldwide broadband stations. The focal mechanism of the 1990 earthquake and its depth, assuming a mean velocity model up to the focal depth, is well constrained by the modelling of Tavera (1991). The modelling of teleseismic seismograms of this earthquake with a spherical earth model gives a thrust mechanism with a small strike-slip component ($\phi = 245°$, $\delta = 63°$, $\lambda = 100°$) while the source duration is four seconds.

We must emphasize the fact that synthetics as well as observed seismograms are ground velocities instead of ground displacement. Synthetic and observed seismograms in fig. 17 show a good agreement at all the stations except at AGD (azimuth 151°), RER (azimuth 153°) and HYB (azimuth 105°): at these three stations the observed amplitude for the *pP* phase is higher than the synthetic one. The *sP* synthetic phase shows a large amplitude only at the station AGD while observed *sP* phases are in good agreement with synthetic amplitude calculated in a spherical

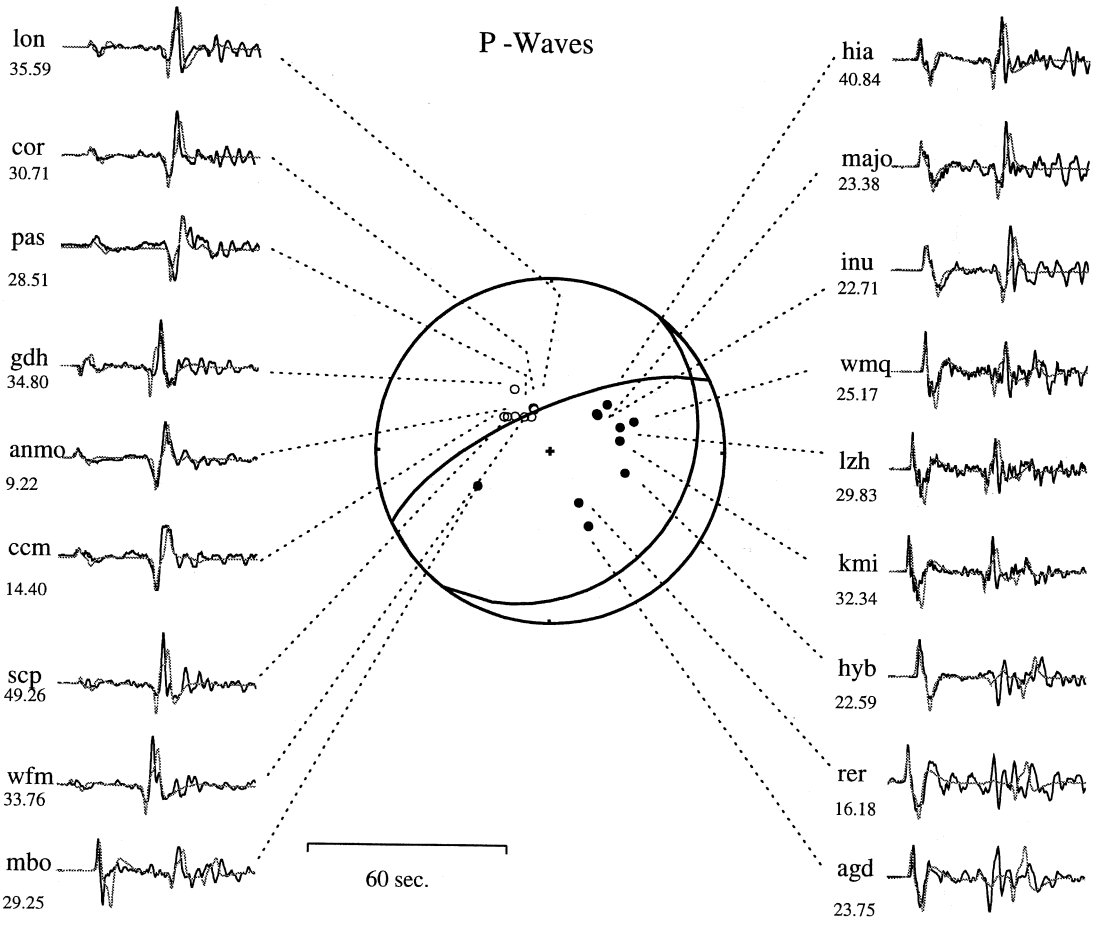

Fig. 17. Comparison of observed and synthetic *P*-wave seismograms of the Rumanian earthquake for a point-source model and for a spherically symmetric Earth.

model for the other two stations. Nevertheless, all the *sP* phases arrived too early in the synthetic seismograms at these three stations. The take-off angles of the *pP* phase are located near the nodal plane, providing a very low amplitude as shown in fig. 18.

As the focal mechanism is very well constrained by 15 stations (fig. 17), the anomalous amplitude on *pP* and *sP* synthetic phases is likely to be an effect of the structure surrounding the source, an effect which might change the take-off angles of these reflected phases. The intermediate depth of this event and its relatively small magnitude make it a very good candidate for a clear observation of the effects of the near-source structure. No other arrivals like *PcP* could significantly modify seismograms in this time window.

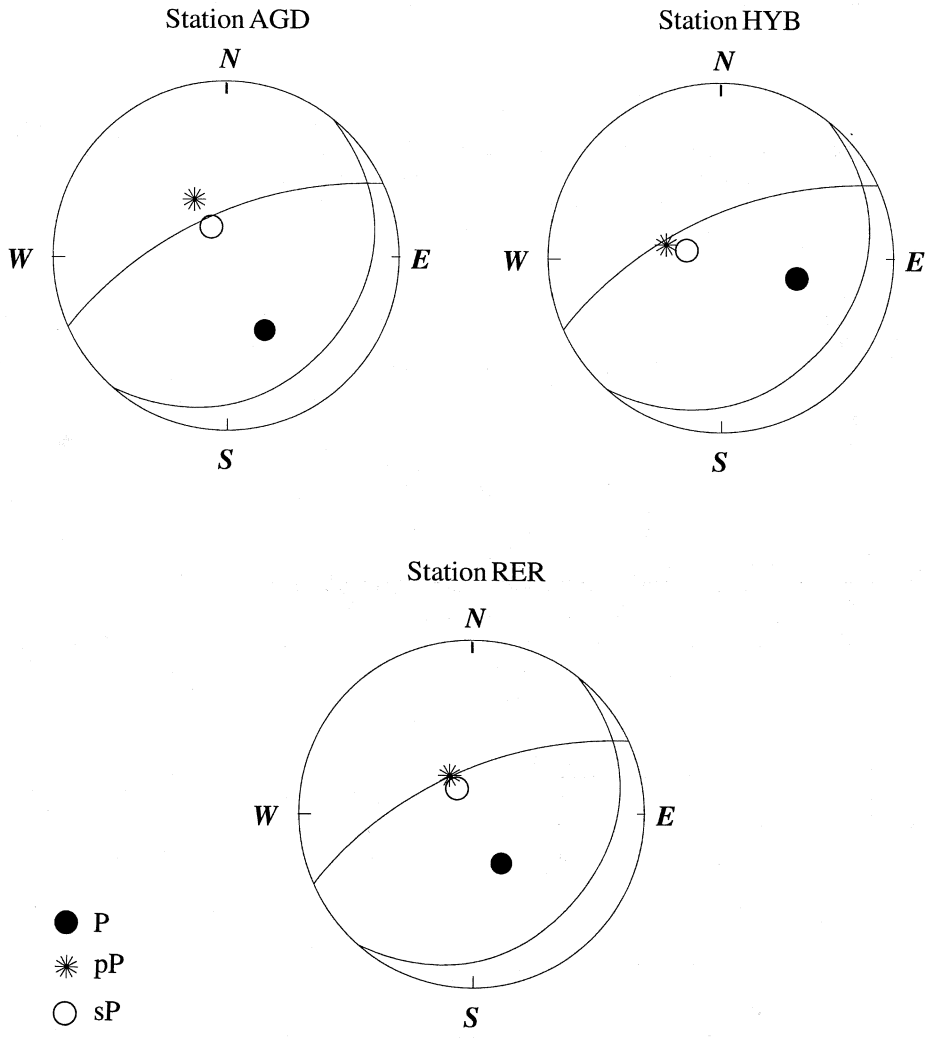

Fig. 18. Take-off angles for *P*, *pP* and *sP* phases for a spherical model of the Earth.

Because the anomalous amplitudes are quite large, heterogeneities must significantly change the ray parameters corresponding to these stations. The hitting point on the focal sphere for rays arriving at these stations should be moved into portions of the radiation pattern with high amplitudes.

In a first attempt, Perrot *et al.* (1994) tried to model the effect of a paleo-subduction zone in the Vrancea region (Onescu, 1986) where the source took place at 90 km. The fit in seismograms did not improve even when a slab curvature was introduced for focusing waves. The anomalous effects have a more superficial origin. The Carpathian arc, where the Vrancea region is located, is surrounded by the Transylvanian and Pannonian basins to the West and by the Moesian basin to the East (see fig. 19). These sedimentary basins are wide (over 70 km) and their depth might be greater than 10 km in the area (Radulescu and Sandulescu, 1973).

The introduction of sedimentary layers enables us to perform a better fit of the observed seismograms as shown at the bottom of fig. 20 with new phases having take-off angles given on the top of the figure. Structures imaged by ray-tracing are described in fig. 21.

To fit the large amplitude of the observed *pP* phase, a dipping interface of 20° in the east direction, separating a sedimentary layer with a constant velocity of 4.6 km^{-1} and a granitic layer with a velocity of 6.5 km^{-1} simultaneously provides a shift of the take-off angles making a more important radiation pattern and an amplification of the Green function, as shown on the bottom of fig. 21.

The *sP* phase has no amplitude when it passes through this dipping interface. This is why the *sP* phase follows the standard ray path with the planar interface in the 2-D Cartesian model we used, describing a sedimentary basin with 7 km of depth to the west of the dipping interface, necessary to fit the *sP* phase in time. For the amplitude of the *sP* phase at AGD, another sedimentary layer 1 km deep with a velocity of 2.5 km^{-1} was necessary for the *P* wave below the surface to fit the lower amplitude of the observed *sP* phase.

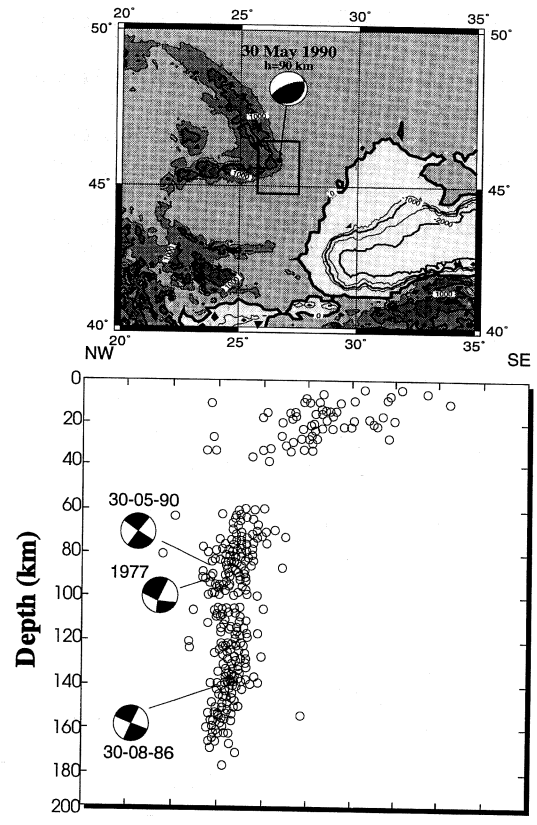

Fig. 19. Maps of tectonics and seismicity in the Vrancea area: a Benioff plane explains the important depth of the 1990 studied earthquake. Two previous shocks, the 1986 event as well as the 1977 event, are also very deep. This depth allows separation between direct pulses and reflected waves on superficial sedimentary basins.

Finally, these interfaces introduce supplementary reflections: the *sd*1*P* and the *pd*1*P* phases reflected at the bottom of the sedimentary basin and the *pd* 2*P* phases reflected at the bottom of the shallow sedimentary basin (see fig. 21). We must also include the synthetic *PcP* phase, reflection from the external core.

We deduced a hypothetical model to fit the observed seismograms at these three stations. This model is still not perfect but improves the modelling compared to the spherical model.

Local information should be obtained to check the consistency of such a model.

This peculiar deep event showed evidence of strong effects of the structure near the source. The source time function of this event is very simple and allows us to analyze ground velocities instead of displacements. In case of complex events, could we manage to fit ground velocities instead of displacements? We want to apply this procedure to another earthquake occurring in the same general area, a complex event under a highly heterogeneous basin.

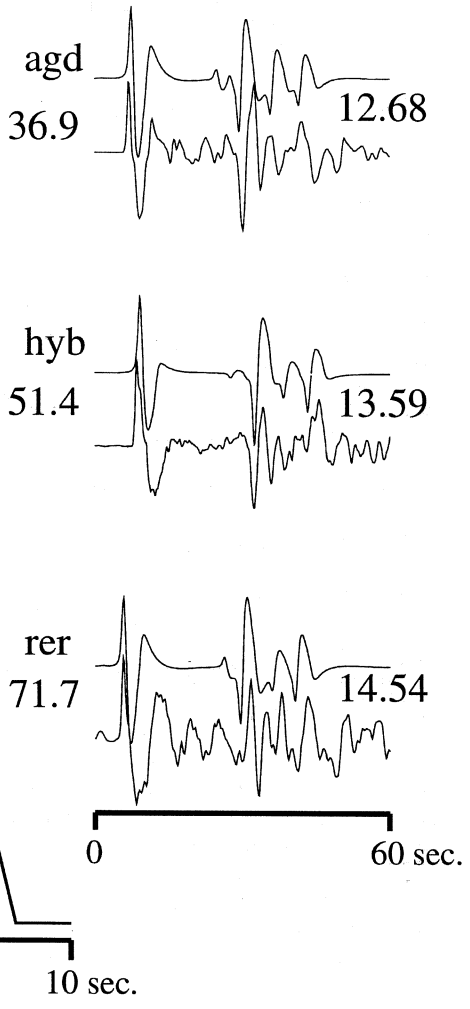

Fig. 20. Synthetic and observed seismograms at the three stations showing anomalous phases when reflected waves are included.

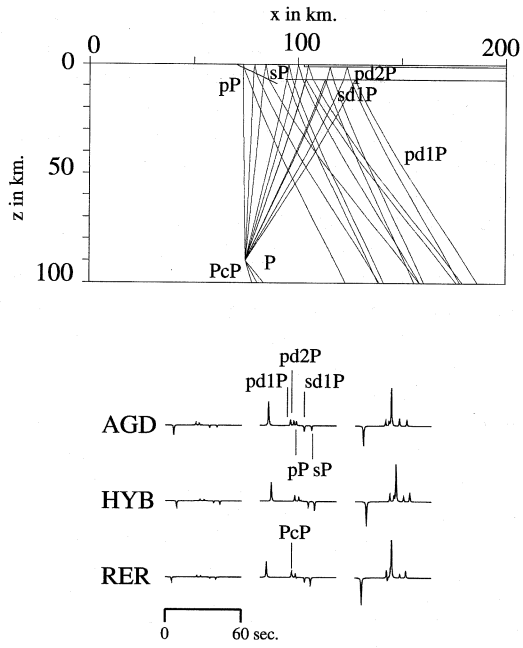

Fig. 21. Sampling of the medium around the source by rays and associated Green functions to estimate their respective importances: the use of ray method makes interpretation easier for the seismologist.

6. The Erzincan earthquake of March 13, 1992 (M_S = 6.2)

The March 13, 1992 Erzincan, Turkey earthquake occurred in the eastern part of Turkey where the North Anatolian fault produces a secondary Northeast Anatolian fault. This strike-slip event with no obvious rupture breaking (Barka and Eyidogan, 1993) is located below the Ercinzan basin, a poorly consolidated basin. Aftershocks were located in a southeast direction compared to the main shock.

In a first check of source focal mechanisms, we proceeded to fit observed displacements at many broadband stations (fig. 22) using the method proposed by Nábělek (1984). Seismograms were band-pass filtered between 0.01 Hz and 0.2 Hz and converted to the same distance. We consider the point-source approximation and introduce a poorly consolidated basin 3 km deep with a P wave velocity of 1.60 kms^{-1} and S wave velocity of 0.48 kms^{-1}. The focal mechanism we obtained is ($\phi = 119°$, $\delta = 79°$, $\lambda = -170°$) while the source duration is 12 s with two main bursts of energy. The depth is not well constrained and has been fixed at 9 km.

Synthetic and observed seismograms are displayed in fig. 22 and show the influence of the basin on small phase wiggles behind the first pulse. These converted phases were not strong enough to be able to interpret later picks and a new source with a time delay of 10 s is required. A detailed analysis of this earthquake is possible with the introduction of multiple sources. At the same time, a better knowledge of the sedimentary basin will avoid the introduction of ghost images of important subevents such as small subevent. The trade-off between the influence of the rupture and the influence of the near-source medium are difficult to separate using displacement seismograms.

Is the ground velocity more sensitive to structural features and rupture complexity? Comparison between synthetic and observed seismograms (fig. 23) for the same source obtained previously by the inversion procedure shows us that the overall fit is performed while slightly shifting time delays of specific phases might dramatically improve the fit of these velocity seismograms. We think it is possible in a trial-and-error attempt to introduce a model of basin that makes synthetic and observed velocity seismograms nearly identical. That is the subject of current research.

7. Discussion and conclusions

We have presented four studies of earthquakes sharing approximately the same azimuthal coverage with respect to worldwide

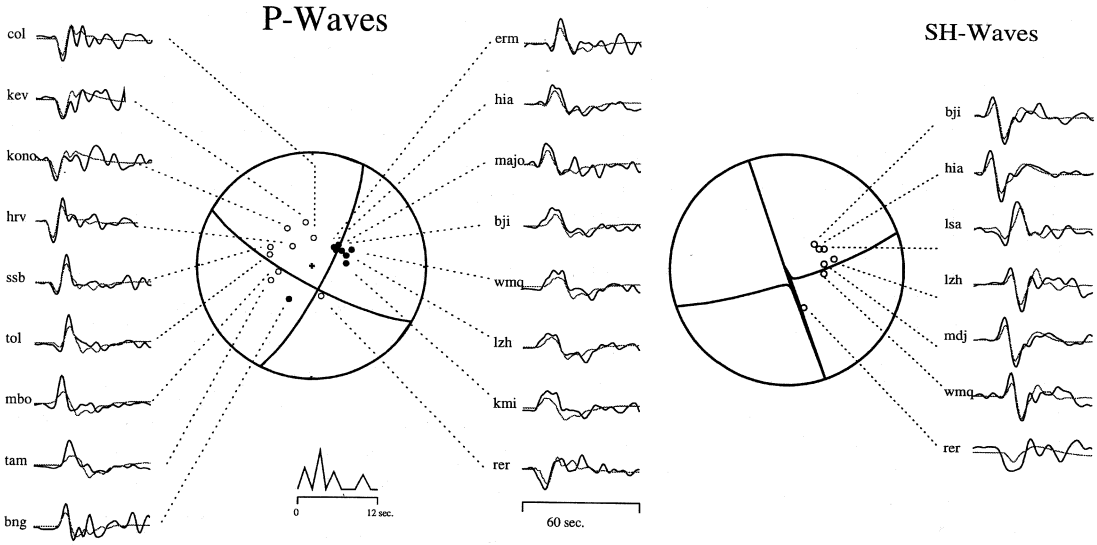

Fig. 22. Comparison between ground displacement synthetics and observed seismograms for a point-source model for the Erzincan earthquake.

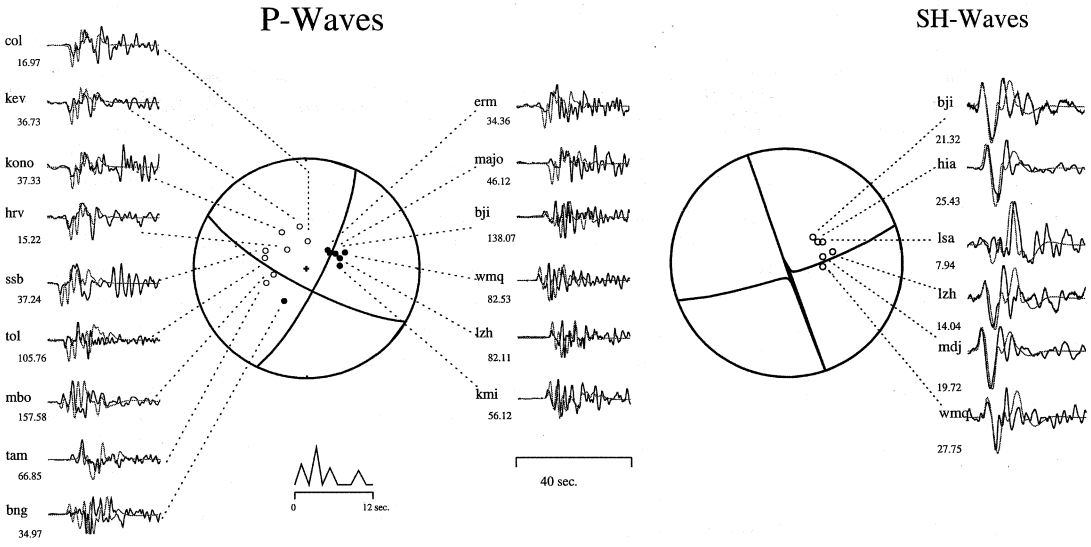

Fig. 23. Comparison between ground velocity synthetics and observed seismograms for a point-source model for the Erzincan earthquake. Note the appearing complexity of these velocity seismograms. The teleseismic information has not been fully extracted.

broadband stations. For these earthquakes, seismograms recorded at teleseismic stations show both the signature of the focal mechanism and of the medium surrounding the source. The relative importance of these two effects depends on the earthquake.

Although the focal mechanism dominates the wave shape of seismograms, seismologists arrive at such a detailed analysis of the rupture process that some caution should be stressed and the influence of the medium better estimated. In order to do so, tools for modelling the wave propagation accurately around the source have been developed.

These tools based on ray tracing techniques still have the advantage of being very efficient in terms of computer CPU time. Simple analysis of phases independently is possible and allows us to analyze seismograms precisely. Moreover, the extension to 3-D geometry is a current line of research.

In this paper, we have attempted to find source and medium parameters by trial and error. It is worth mentioning that inversion methods have to be used. The linearized approach used for example to estimate focal mechanisms of earthquakes (Nábělek, 1984) allows one to investigate the model space locally but, for the new model including both source and the medium parameters, other techniques of inversion might be investigated such as global grid search or simulated annealing methods in order to escape from local minima. This will be a subject of ongoing research.

In inversion procedures to estimate earthquake mechanism parameters, one might modify the frequency content of seismograms, going from relatively low-frequency ground displacement up to higher-frequency ground velocity. It is the same trend as when seismologists try to interpret WWSSN SP seismograms which are a higher-frequency content than WWSSN LP seismograms. There is certainly a limit to this increase in the frequency content: accelerograms seem at the present time more difficult to analyze. The limit we can think about is related to the capabilities of transporting the energy over large distances without a complete distortion of the signal. A

limit around 0.5 Hz seems to be reasonable for teleseismic studies.

Applications to the different earthquakes demonstrate that the increasing number of broadband stations might be enough now to reach this target of a completely seismological independent definition of the rupture process and of the medium surrounding the source from teleseismic data. Therefore, field observations can now be used to check the consistency with the seismological data.

Acknowledgements

This paper has benefitted from many discussions with Véronique Farra and Raùl Madariaga. John Nábělek provided his computer program for inversion of source parameters by synthesizing ground displacement. Michael Hamburger critically review this manuscript. This work was partially supported by INSU-CNRS through the tomography group.

REFERENCES

AKI, K. and P. RICHARDS (1980): *Quantitative seismology: theory and methods* (W. H. Freeman & Co), 50-70.

ANDERSON, D. and R. HART (1978): Attenuation models of the earth, *Phys. earth, Planet. Int.*, **16**, 289-306.

BARKA, A. and H. EYIDOGAN (1993): The Erzincan earthquake of 13 march 1992 in Eastern Turkey, *Terra Nova*, **5**, 190-194.

BURRIDGE, R. (1976): *Some mathematical topics in seismology* (Courant Institut of Mathematical Sciences, New York University Press), pp. 317.

CAMPOS, J., R. MADARIAGA, J. NÁBĚLEK, B. BUKCHIN and A. DESCHAMPS (1994): A faulting process of the 1990 June 20 Iran earthquake from broad-band records, *Geophys. J. Int.*, **118**, 31-46.

CARPENTER, E. and E. FLINN (1965): Attenuation of teleseismic body waves, *Nature*, **207**, 745.

ČERVENÝ, V. and J. JANSKÝ (1983): Ray amplitude of seismic body waves in homogeneous radially symmetric media, *Stud. Geophys. Geod.*, **27**, 9-18.

CHAPMAN, C. (1978): A new method for computing seismograms, *Geophys. J. R. Astr. Soc.*, **54**, 481-518.

CISTERNAS, A., H. PHILIP, J. BOUSQUET, M. CARA, A. DESCHAMPS, L. DORBATH, C. DORBATH, H. HAESSLER, E. JIMENEZ, A. NERCESSIAN, L. RIVERA, B. ROMANOWICZ, A. GVISHIANI, N. SHEBALIN, I. APTEKMAN, S. AREFIEV, B. BORISOV, A. GORSHKOV, V. GRAIZER, A. LANDER, K. PLETNEV, A. ROGOZHIN and R. TATEVOSSIAN (1989): The Spitak (Armenia) earthquake of 7 december 1988: field observations, seismology and tectonics, *Nature*, **339**, 675-679.

FARRA, V., J. VIRIEUX and R. MADARIAGA (1989): Ray perturbation theory for interfaces, *Geophys. J. Int.*, **99**, 377-390.

FUCHS, K. and G. MÜLLER (1971): Computation of synthetic seismograms with the reflectivity method and comparison of observations, *Geophys. J. R. Astr. Soc.*, **23**, 417-433.

GAFFET, S. (1995): Teleseismic waveform modeling including geometrical effects of superficial geological structures near to seismic sources, *Bull. Seismol. Soc. Am.* (in press).

GIVEN, J. W. and D. V. HELMBERGER (1980): Upper mantle structure of Northwestern Eurasia, *J. Geophys. Res.*, **85**, 7183-7194.

HAESSLER, H., A. DESCHAMPS, H. DUFUMIER, H. FUENZALIDA and A. CISTERNAS (1992): The rupture process of the Armenian earthquake from broad-band teleseismic body wave records, *Geophys. J. Int.*, **109**, 151-161.

HASKELL, N. (1964): Radiation pattern of surface waves from point sources in a multi-layered medium, *Bull. Seismol. Soc. Am.*, **54**, 377-394.

HASKELL, N. (1966): Total energy and energy spectral density of elastic wave radiation from propagating faults, *Bull. Seismol. Soc. Am.*, **56**, 125-140.

HASKELL, N. (1969): Elastic displacements in the near-field of a propagating fault, *Bull. Seismol. Soc. Am.*, **59**, 865-908.

HELMBERGER, D. (1968): The crust-mantle transition in the Bering sea, *Bull. Seismol. Soc. Am.*, **58**, 179-214.

JACKSON, D. (1979): The use of a priori data to resolve non-uniqueness in linear inversion, *Geophys. J. R. Astr. Soc.*, **57**, 137-157.

KENDALL, J. and C. THOMSON (1993): Seismic modelling of subduction zones with inhomogeneity and anisotropy. 1. teleseismic *P*-wavefront tracking, *Geophys. J. Int.*, **112**, 39-66.

KIKUCHI, M. and H. KANAMORI (1982): Inversion of complex body waves, *Bull. Seismol. Soc. Am.*, **72**, 491-506.

KIKUCHI, M., H. KANAMORI and K. SATAKE (1993): Source complexity of the 1988 Armenian earthquake: evidence for a slow after-slip event, *J. Geophys. Res.*, **23**, 240-252.

NÁBĚLEK, J. (1984): Determination of earthquake source parameters from inversion of body waves, *Ph.D. Thesis*, MIT, Cambridge, Massachusetts, pp.361.

OKAL, E. (1992): A student's guide to teleseismic body wave amplitudes, *Seismol. Res. Lett.*, **63**, 169-180.

OKAMOTO, T. and T. MIYATAKE (1989): Effects of near source seafloor topography on long-period teleseismic *P* waveforms, *Geophys. Res. Lett.*, **16**, 1309-1312.

ONESCU, M. (1986): Some source and medium properties of the Vrancea region, Romania, *Tectonophysics*, **126**, 245-258.

OWENS, T.J. and R.S. CROSSON (1988): Shallow structure effects on broadband teleseismic *P* waveform, *Bull. Seismol. Soc. Am.*, **78**, 96-108.

PACHECO, J., C. ESTABROOK, D. SIMPSON and J. NÁBĚLEK (1989): Teleseismic body wave analysis of the 1988 Armenian earthquake, *Geophys. Res. Lett.*, **16**, 1425-1428.

PAPADIMITRIOU, P. (1988): Ètude de la structure du manteau

supérieur de l'Europe par modélisation des ondes de volume engendrées par des séismes égéens, *Thèse*, Université de Paris 7.

PAULSSEN, H. (1988): Evidence for a sharp 670-km discontinuity as inferred from *P* to *S* converted waves, *J. Geophys. Res.*, **93**, 10489-10500.

PERROT, J., A. DESCHAMPS, V. FARRA and J. VIRIEUX (1994): Azimuthal distorsion of the seismic focal sphere: application to earthquakes in subduction zone, *Phys. Earth Planet. Int.*, **84**, 247-270.

PHILIP, H., A. CISTERNAS, A. GVISHIANI and A. GORSHKOV (1989): The Caucasus: an example of the inital stages of continental collision, *Tectonophysics*, **161**, 1-21.

RADULESCU, D. and M. SANDULESCU (1973): The plate-tectonics concept and geological structure of the Carpathians, *Tectonophysics*, **16**, 155-161.

RUFF, L. (1980): Seismicity and the subduction process, *Phys. Earth Planet. Int.*, **23**, 240-252.

TARANTOLA, A. and B. VALETTE (1982): Inverse problems = quest for information: *J. Geophys.*, **50**, 159-170.

TAVERA, J. (1991): Études des mécanismes focaux de gros séismes et sismicité dans la région de Vrancea-Roumanie, *Rapport de stage de DEA de Géophysique interne*, IPGP, Paris.

VIRIEUX, J. and V. FARRA (1991): Ray tracing in 3-D complex isotropic media: an analysis of the problem, *Geophysics*, **16**, 2057-2069.

WIENS, D. (1989): Bathymetric effects on body waveforms from shallow subduction zone earthquakes and application to seismic processes in the kurile trench, *J. Geophys. Res.*, **94**, 2955-2972.